PCCP

PAPER

View Article Online
View Journal | View Issue

Cite this: *Phys. Chem. Chem. Phys.*, 2016, **18**, 29330

Lattice strain effects on doping, hydration and proton transport in scheelite-type electrolytes for solid oxide fuel cells†

Chiara Ferrara,[a] Christopher Eames,[b] M. Saiful Islam[b] and Cristina Tealdi*[a]

Received 16th September 2016,
Accepted 29th September 2016

DOI: 10.1039/c6cp06395k

www.rsc.org/pccp

Lattice strain is considered a promising approach to modulate the structural and functional properties of oxide materials. In this study we investigate the effect of lattice strain on doping, hydration and proton transport for the family of scheelite-type proton conductors using both atomistic and DFT computational methods. The results suggest that tensile strain improves the dopant solubility and proton uptake of the material. The anisotropic proton pathways change from being within the *a*–*b* plane to being in the *a*–*c* plane. However, the predicted reduction in the migration barrier suggests that improvements in ionic conductivity due to lattice strain effects will be limited, in contrast with the work on oxide ion conduction. Such results are rationalized in terms of structural changes and differences in migration steps between oxide ions and protonic species.

1. Introduction

Proton conducting oxides have received considerable attention over the past few decades in view of their potential to lower the solid oxide fuel cell (SOFC) operating temperature to an intermediate-to-low temperature range.[1–3] Such a decrease in the operating temperature would improve the chemical and mechanical stability of the SOFCs and reduce their cost. Decreasing the operating temperature while maintaining the high ionic conductivity target of the electrolyte layer (10^{-2} S cm^{-1}) and the rapid surface oxygen exchange kinetics at the cathode requires the development of novel functional materials or a significant optimization of the existing systems.[4]

With regard to the electrolyte layer, the reference class of compounds for proton conducting SOFCs is the family of doped perovskites with a general formula ABO_3 (A = Ca, Sr, Ba; B = Ce, Zr). Proton conduction in this system was reported during the 1980s by Iwahara *et al.*,[5] with conductivities reaching 0.01 S cm^{-1} at 400 °C for doped $BaZrO_3$.[6] Major problems associated with the use of perovkite-type proton conductors are the low chemical stability in the CO_2 containing atmosphere and the difficult sinterability.[2] To overcome this drawback, several classes of oxides have been proposed.[1,7]

One of the latest family of oxides proposed is the *ortho*-niobate and *ortho*-tantalate class of compounds with a general formula $LnXO_4$ (Ln rare earth, X = Nb, Ta).[8,9] This family of oxides is characterized by the presence of a phase transition between the low temperature fergusonite-type structure and the high temperature scheelite-type polymorph.[10] The best reported conductivity values are obtained for the 1% Ca doped $LaNbO_4$ composition, reaching reasonable values of 10^{-3} S cm^{-1} at 950 °C in a wet atmosphere.[8]

Different strategies have been proposed for further improvement of the transport properties of these *ortho*-niobates. As the conductivity depends on the concentration of the charge carriers, different dopants were tested but the solubility limit for Ca^{2+} on the La^{3+} site is found to be in the 0.5–1.0% range.[11] Doping on the B site was also considered, but the dopant solubility is also low and in general the activation barrier for proton migration for the B-site doped materials is higher than the A-site doped systems.[12] Therefore, although several compositions and combinations of dopants were considered, no dramatic improvement of the ionic conductivity was achieved.[7,13–17] This "chemical approach", based on the search for novel compositions or better dopants, has represented the driving path for the optimization of the transport properties of ionic conducting materials for decades.

A more "physical approach", based on the exploitation of lattice strain effects on the transport properties of ionic conducting materials, is currently acquiring growing interest.[18] In this regard, computational and experimental studies have focused on electrolytes[19–22] as well as cathode materials[23,24] for SOFCs based on oxide-ion conduction. In general, it has been shown that lattice strain effects can improve the transport properties of oxide ion conductors by several orders of magnitude, as a

[a] *Department of Chemistry, University of Pavia and INSTM, Viale Taramelli 16, 27100 Pavia, Italy. E-mail: cristina.tealdi@unipv.it*
[b] *Department of Chemistry, University of Bath, Bath, BA2 7AY, UK*

† Electronic supplementary information (ESI) available: Table of potential parameters, calculated density of states and energy barriers profile obtained from NEB calculation. See DOI: 10.1039/c6cp06395k

consequence of structural modifications. For example, computational studies on the fluorite-structure oxide ion conductors have suggested the possibility of increasing the ionic conductivity by a factor of 10^4–10^6 within the strained system,[19,20] and thin films of $La_{0.6}Sr_{0.4}CoO_{3-\delta}$ have been reported with oxygen diffusivity values of two orders of magnitude higher compared to the bulk material.[23] Similar promising results have been obtained and predicted for K_2NiF_4-type cathode materials[25] and perovskite-type electrolytes.[21] In contrast, the same approach has received very limited attention in the field of proton conducting SOFCs, with a computational study devoted to the investigation of biaxial strain effects on the proton conductivity of Y-doped $BaZrO_3$ through reactive molecular dynamics.[26] This study suggests that moderate biaxial strain can slightly improve proton diffusivity in perovskite-type materials.

In this work, we present a computational investigation of the influence of biaxial strain on dopant solubility, hydration energetics and proton migration for the scheelite-type $LaNbO_4$ system. The application of biaxial strain mimics the situation of strained epitaxial films where the strain is induced by a lattice mismatch at the interface with the substrate. The results presented are therefore relevant to the preparation of micro-SOFCs. In addition, this study aims to expand the set of systems explored in the application of strain engineering as a strategy to modulate the functional properties of materials in solid state thin film devices.

2. Computational methods

The atomistic energy minimization and DFT methods employed in this study have been presented extensively elsewhere.[27,28] In this study static lattice simulations were performed according to the energy minimization procedure embodied in the GULP code.[29] The interaction between ions was modelled with Buckingham pair potentials. Electron polarizability was described by the shell model.[30] Lattice relaxation after the introduction of a charged point defect was treated according to the Mott–Littleton method.[31] The set of potential parameters used in this study (Table S1 of the ESI†) was already optimized and used for the description of the tetragonal unstrained $LaNbO_4$ system.[32] The O–H interaction has been described with the use of the well-established Morse potential (Table S2 in the ESI†) already used in other proton conducting oxides.[33–35] Within the GULP code, lattice strain in the −3% to +3% range of the unstrained relaxed cell parameters was applied simultaneously along the *a* and *b* directions while the third cell parameter and all the atomic coordinates were allowed to relax. Calculations were performed in the *P*1 space group, to allow for possible lowering of the symmetry upon the imposition of lattice strain.

The DFT-based calculations were performed with the VASP code[36] using projector augmented wave (PAW) pseudopotentials and the PBE exchange correlation functional term proposed by Perdew *et al.*[37] The energy cut-off was set at 600 eV and the unit cells (both strained and unstrained) were optimized until the residual forces were less than 0.005 eV $Å^{-1}$ and the total energy difference less than 0.005 eV using an 8 × 8 × 4 *k*-point grid. In this case, for the strained systems, −3% and +3% strain compared to the relaxed lattice parameters for the unstrained system were applied simultaneously along the *a* and *b* directions. Full relaxation of the atomic coordinates was then achieved for different values of the *c* lattice parameter, so as to find the one associated to a minimum in the total energy of the unit cell (see Fig. S1 for details, ESI†).

The energetics of proton transport were calculated using the DFT-based nudged elastic band (NEB) method. For these NEB calculations, 2 × 2 × 1 supercells containing a single proton were employed. The NEB calculations were performed using the climbing image method[38] and considering different numbers of images according to the complexity of the migration paths. The *k*-point grid was reduced to 2 × 2 × 2 while maintaining the energy cut-off at 600 eV.

3. Results and discussion

3.1 Structural modelling

The tetragonal scheelite-type structure of $LaNbO_4$ (space group *I*4/1*a*), presented in Fig. 1, consists of isolated NbO_4 tetrahedral units separated by La^{3+} ions. We first turn our attention to the effect of applied strain on the scheelite structure. Fig. 2 shows the calculated volume and lattice parameters as positive and negative strains are applied. In general, and as usually observed for oxide materials, as a positive strain is applied biaxially in the *a*–*b* plane the *c* lattice parameter is observed to contract whereas overall the volume slightly increases. When negative strain is applied the *c* lattice parameter increases but the volume slightly decreases. We note the excellent agreement between the unstrained experimental lattice parameters and volume and those calculated by both computational techniques. Furthermore, both computational techniques show the same magnitude of *c* parameter variation as strain is applied. All of this supports the validity of the models and the stability of the structure under the applied strain conditions.

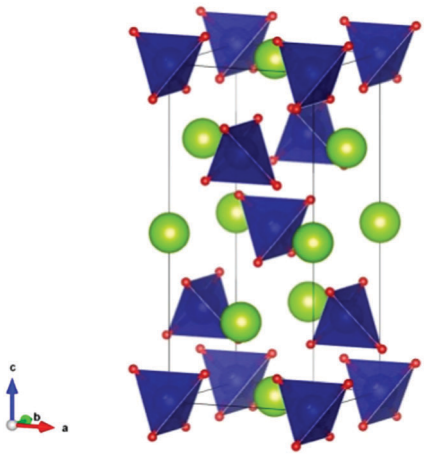

Fig. 1 Scheelite crystal structure of $LaNbO_4$. Nb^{5+} (blue) ions are forming NbO_4 units separated along the three dimensions by La^{3+} (green) ions in four-fold coordination with oxygen (red).

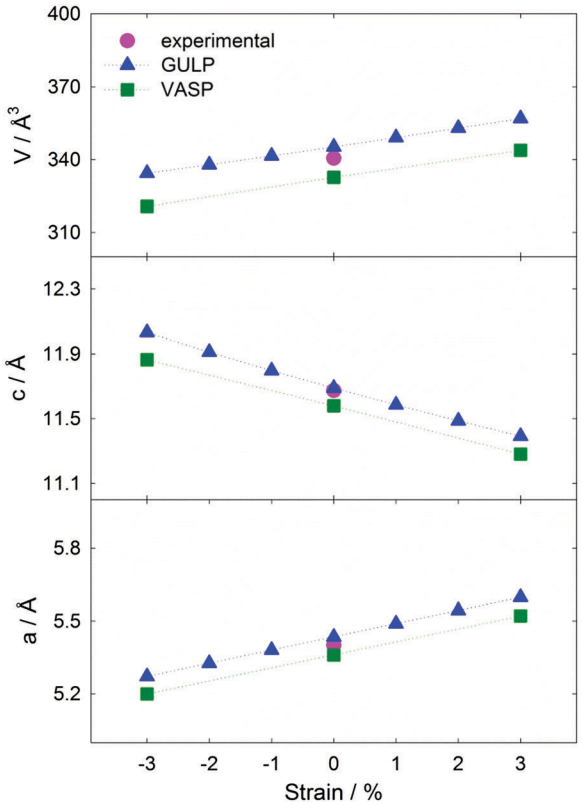

Fig. 2 Experimental[39] and calculated structural parameters and cell volume for the tetragonal $LaNbO_4$ structure under various applied biaxial strains in the *a*–*b* plane.

Structural analysis of the calculated results indicates that when the strain is applied in the *a*–*b* plane the tetragonal symmetry is maintained and the NbO_4 tetrahedra are undistorted; the Nb–O bond lengths respond linearly to the applied strain (see Fig. S3, ESI†). Since Nb^{5+} has a d^0 electronic structure there are no crystal fields or magnetic effects to encourage asymmetric distortions of the tetrahedra. In addition, the density of states (DOS) obtained from our DFT calculations are in good agreement with the DOS previously reported for the same structure when no strain is applied[40] (Fig. S2 of the ESI†).

We recall that the $LaNbO_4$ system is characterized by a phase transition between a monoclinic room temperature fergusonite-type structure and a tetragonal high temperature scheelite-type structure at around 500 °C.[10] As the high temperature phase is the best proton conductor, low-temperature stabilization of the scheelite phase is desirable. In addition, the presence of a phase transition within the operating temperature regime is always considered detrimental for practical applications. Successful results have been recently reported for the room temperature deposition of $La_{0.99}Ca_{0.01}NbO_4$ films with the scheelite structure.[41] The inversion of the phase stability between the fergusonite and scheelite polymorphs has been ascribed in that case to the nanostructured nature of the film in combination with a suitable substrate. At the same time, the deposition of epitaxial fergusonite-type films of $La_{0.995}Ca_{0.05}NbO_{4-\delta}$ by PLD on (110)-oriented $NdGaO_3$ has been reported.[42] In this case, a decrease of transition temperature of more than 200 °C compared to the corresponding bulk system was reported, supporting a considerable reduction of the monoclinic distortion in the epitaxial films. These results suggest that with the right combination of substrate type and deposition conditions it is possible to deposit epitaxial scheelite-type strained films. For these reasons this study focuses on the tetragonal scheelite-type polymorph.

3.2 Hydration and Ca-doping

The mechanism through which protons are introduced into an oxide structure is accepted to be substantially the same for all host systems.[43,44] Oxides can accommodate a certain concentration of protons *via* the incorporation of H^+ ions generated by the dissociative absorption of water molecules from the gas phase. The OH^- group can fill an oxygen vacancy, while the H^+ ion obtained from the dissociation directly bonds to a lattice oxygen position. The overall reaction can be expressed using the Kröger–Vink notation, as follows:

$$H_2O_{(gas)} + V_O^{\bullet\bullet} + O_O^{\times} \leftrightarrow 2OH^{\bullet} \quad (1)$$

Strain may affect the energetics of proton incorporation. To examine this, we have calculated the hydration enthalpy as a function of strain according to eqn (1), and the results are shown in Fig. 3. The hydration enthalpy shows a clear decrease with increasing strain, suggesting a positive effect of tensile strain on the amount of water incorporation within the system. This trend reflects the changes in the formation energies of the OH group and the oxygen vacancies, both of which become more favourable as tensile strain is applied (Fig. S4, ESI†). Such changes in defect formation energy reflect structural rearrangements due to the presence of defects.

The presence of oxygen vacancies in the crystal is generally obtained through doping with acceptor dopant species. For $LaNbO_4$, the most successful way to introduce oxygen vacancies that can be filled by protonic species is the substitution of La^{3+} with Ca^{2+},[9,11] according to the following equation:

$$CaO + La_{La}^{\times} + \frac{1}{2}O_O^{\times} \rightarrow Ca_{La}^{'} + \frac{1}{2}La_2O_3 + \frac{1}{2}V_O^{\bullet\bullet} \quad (2)$$

However, the low solubility of dopant ions that is experimentally observed in the scheelite structure prevents any conductivity enhancement through doping.[11,45] In our study, in order to

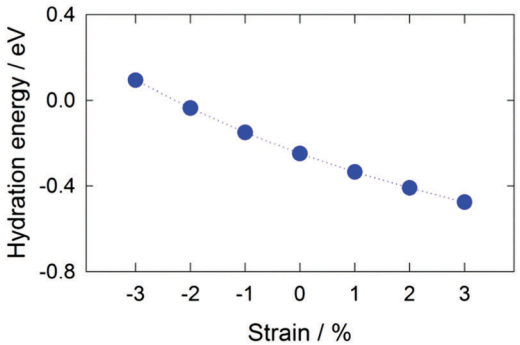

Fig. 3 Calculated hydration energies as a function of applied strain.

determine if the application of strain improves the solubility of dopants, we have evaluated the solution energies of Ca^{2+} in $LaNbO_4$ as a function of the imposed strain. The calculated solution energy decreases with the applied strain, from 1.25 eV for the unstrained system to 1.05 eV for the 3% tensile strained system. Such a decrease in solution energy suggests that it is possible to dope a higher concentration of Ca^{2+} into tensile strained crystals, which would enhance the proton transport properties of scheelite $LaNbO_4$.

Another important aspect of extrinsic doping is the possibility of binding of dopant ions to mobile defects. Due to their opposite charge, oxygen vacancies introduced by the extrinsic doping can associate with the dopant ions, forming a cluster; this effect has been widely observed and described for oxygen ion conductor materials.[46] Dopant ions can also trap migrating proton species.[43] The clustering effect in Ca-doped $LaNbO_4$ has been evaluated by comparing the energy of the simple bi-component cluster system where the M′ ion is placed in the first coordination sphere of the $V_O^{\bullet\bullet}$ (or the $OH^{\bullet}$ group) and the sum of the corresponding isolated defects according to the formula:

$$E_{\text{bind}} = E_{\text{cluster}} - \sum E_{\text{isol.def.}} \quad (3)$$

with this convention, negative values of binding energy imply that the dopants and defects are bound and the cluster is more stable than the isolated defects. This approach has been widely applied to the estimation of binding energy terms for the oxide ion and proton conducting oxides, successfully reproducing experimental trends in their conduction properties.[47] Our calculations show that strain lowers the binding energy of defect clusters; the binding energy of the Ca^{2+}–OH^- pair cluster reduces from −0.25 eV for the unstrained system to −0.18 eV for the 3% tensile strained system. Similarly, the Ca^{2+}–oxygen vacancy pair cluster is predicted to be less bound in the 3% tensile strained system, with binding energies lowered from −0.91 eV to −0.77 eV.

The formation of a cluster involving a mobile defect leads to an increase of the migration barrier. Binding energies between dopant ions and protonic species are therefore considered detrimental for application since they reduce proton mobility in the system.[43,48] At the same time, trapping of the oxygen vacancies is expected to decrease the proton concentration, by adding an energy term to the enthalpy of hydration.[43] The predicted lowering of the binding energy effects in tensile strained $LaNbO_4$ suggests a higher mobility of the proton species if tensile strain is applied, together with an easier incorporation of protonic species in the system. We note that such trapping effects are observed experimentally for high doping levels. As the experimental solubility limit of the dopants in the scheelite structure is very low, the clustering effect might be less significant in this system.

3.3 Proton positions and migration paths

Proton species in oxides are usually associated with oxygen ions, as part of a hydroxyl group. For this reason, different positions around the unique oxygen crystallographic site of the $LaNbO_4$ structure have been explored using DFT. Two distinct

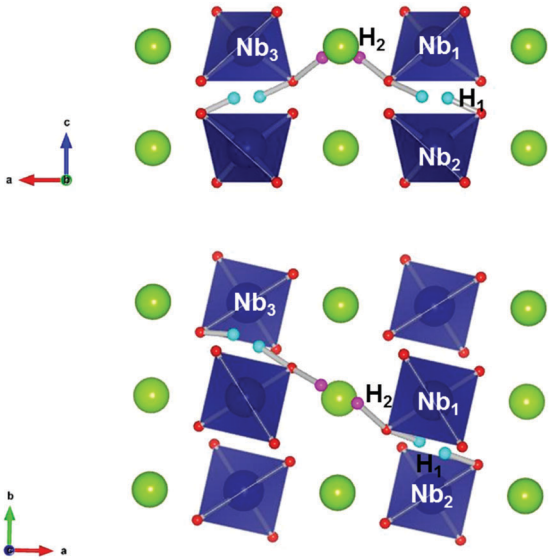

Fig. 4 Stable proton sites in scheelite $LaNbO_4$ – H_1 (cyan) and H_2 (pink) around the NbO_4 tetrahedra (blue, La ions in green). H_1 is more favourable than H_2 in the unstrained crystal.

sites (labelled H_1 and H_2, see Fig. 4) arise as the most favourable, in agreement with previous reports for the unstrained system.[49] The stable proton positions were also evaluated for the +3 and −3% strained cells, in order to see if the relative stability of the two positions is affected by applied strain, as shown in Table 1.

At the H_1 site the proton is bonded to the O of the Nb_1 site and the O–H bond is directed towards the oxygen ion of the nearest NbO_4 units found along the *c* axis (Nb_2 in Fig. 4) and is further stabilized by hydrogen bonds. By contrast, at the H_2 site the O–H bond points in the direction of the nearest La ions along the *a* axis, in the direction of the next neighbour NbO_4 unit within the *a*–*b* plane (Nb_3 in Fig. 4). The position of these two sites remains largely unaffected by the application of the strain, although strain does significantly alter their relative energies, as shown in Table 1. For the negatively strained cell the H_1 site is the most stable position but the energy difference decreases linearly with applied strain so that the two positions are energetically equivalent in the tensile strained system. In all cases the O–H distance is found to be 0.98–1.00 Å, as usually observed in oxides. The presence of stable proton sites at ∼1 Å around the oxygen position has been predicted and observed in $LaNbO_4$ as well as in other proton conductor materials.[49–51]

Starting from these two favourable proton sites, several proton migration routes can be considered. Previous studies on proton conducting oxides have established that the diffusion mechanism is based on two different mechanisms: proton hopping between

Table 1 Energy differences between H_1 and H_2 proton positions as a function of the applied strain

Strain	$E(H_2) - E(H_1)$/eV
−3%	0.23
0	0.15
+3%	0.04

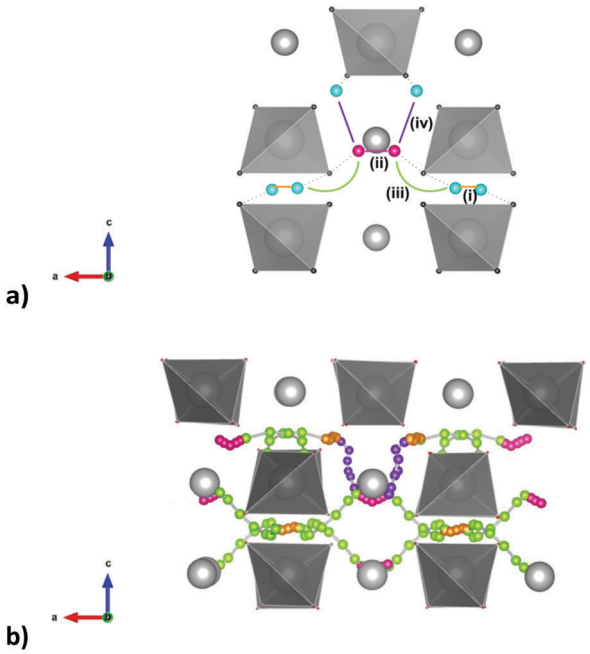

Fig. 5 (a) Schematic representation of the stable proton positions in the tetragonal $LaNbO_4$ structure; NbO_4 tetrahedral units in grey, La ions in light grey. The two proton positions are differentiated with colors: H_1 in light blue, H_2 in pink. (b) Pathways calculated using the DFT-based nudged elastic band method. Colors indicate distinct proton migration events; (i) hops between adjacent H_1 sites in orange, (ii) hops between adjacent H_2 sites in pink, jumps between H_1 and H_2 sites in violet, rotations around the same oxygen ion from the H_1 to H_2 position in green. A combination of (i), (ii) and (iii) results in long range migration in the a–b plane while migration along the c axis requires step (iv).

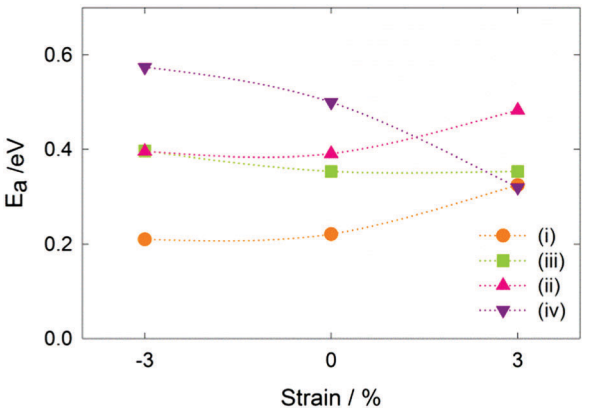

Fig. 6 Energy barriers derived from NEB calculations for the migration steps schematically represented in Fig. 5 referenced with the same labels and color schemes. Migration profiles are reported in Fig S5, ESI.†

two distinct oxygen sites and rotation of the proton ion around an oxygen position. For the scheelite structure four pathways for proton migration between sites are possible, shown in Fig. 5; (i) inter-tetrahedral hops between H_1-sites in the a or b directions, (ii) inter-tetrahedral hops between H_2-sites in the a or b directions, (iii) migration from a H_1 site to a H_2 site (or *vice versa*) *via* rotation of the O–H bond around the tetrahedral edge (iv) inter-tetrahedral hops between H_1 and H_2 sites in the c direction.

In a previous computational study on unstrained scheelite $LaNbO_4$, Fjeld and coworkers found that protons diffuse preferentially in the a–b plane.[49] Proton transfer between H_1 or H_2 sites (type i or ii migration) was calculated to have very low energy barriers (0.04–0.08 eV). The rate determining step for the migration within the a–b plane was found to be the complex type iii migration from a H_1 site to a H_2 site involving a combination of rotation and hopping, with an energy barrier of 0.41 eV. Diffusion along the c axis *via* a type iv jump between H_1 and H_2 sites was found to be very unfavourable, with a much larger activation barrier of 0.74 eV, suggesting strongly anisotropic behaviour with negligible proton conduction in the c direction.

Given that strain alters both the c parameter (and as a result the proton site–site hopping distances) and the proton site energies, it is possible that the proton migration will also be affected by the application of strain. To investigate this we calculated the proton migration energies for all four paths for both strained and unstrained cells (Fig. 6).

First, for unstrained cells, we find the same trend as Fjeld *et al.* discussed above;[49] a large value of 0.51 eV (type iv) for the migration energy along the c-direction, relatively low migration energy for equivalent site hops (type i and ii) and a rate limiting migration energy in the a–b plane of approximately 0.4 eV (type iii). Differences between the calculated values can be ascribed to our use of a more accurate basis set, spin polarization to capture the energetics of unpaired electrons during bond breaking and more images along the NEB path. Nevertheless, the overall prediction remains consistent: anisotropic migration confined to the a–b plane.

Second, for cells compressively strained we find that there is little change for the migration energies in the a–b plane but the migration barrier in the c-direction increases from 0.51 eV to 0.57 eV. Overall, compressive strain would not be expected to influence the proton conductivity other than to exacerbate the already high degree of anisotropy.

Finally, we consider tensile strain. It can be seen in Fig. 6 that there is a significant reduction in the migration barrier along the c-direction from 0.51 eV to 0.32 eV (type iv migration). The rate limiting migration barrier in the a–b plane (type ii hop) increases markedly from 0.39 eV to 0.48 eV. These changes in activation energy can be rationalized by the fact that tensile strain increases the proton site to site distance in the a–b plane and reduces it in the c-direction. The overall effect of tensile strain is to maintain the anisotropic proton diffusion, but to switch it from the a–b plane to the a–c plane, as represented schematically in Fig. 7.

Further atomic-scale analysis reveals that proton migration is accompanied by local rearrangement of the structure involving tilting, rotation or distortion of polyhedra. For the unstrained system, the proton hopping between two H_1 sites presents the lowest activation energy of $\sim$0.2 eV. By contrast hopping between H_2 sites has a higher energy barrier of $\sim$0.4 eV; this difference can be explained by considering the local O–H bonds along the two migration steps. At the saddle point for the H_1–H_1

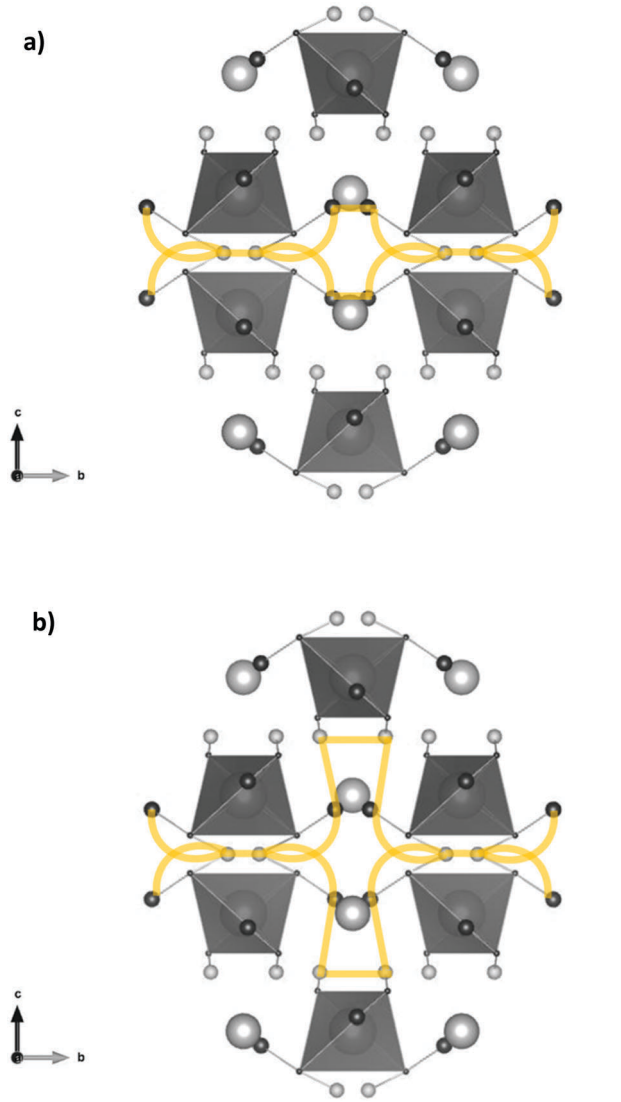

Fig. 7 Schematic representation of long range proton diffusion pathways in (a) unstrained and (b) tensile strained $LaNbO_4$. (NbO_4 tetrahedra – dark grey, La^{3+} – large light grey spheres, H_1 – small light grey spheres, H_2 small dark grey spheres, proton migration pathway – orange).

hop the O–H distances from the initial and final oxygen sites are 1.24 Å and 1.23 Å, whereas for H_2–H_2 hops the O–H distances at the saddle point are 1.55 Å and 1.53 Å, respectively. The increase in the O–H distance and the formal breaking of the O–H bond in H_2–H_2 hops requires a higher energy. Strain alters these energy barriers since it alters the proton site to site distances and directly affects the extent to which the O–H bonds are broken. Further support for this comes from the fact that the 0.36 eV rotational energy barrier around the NbO_4 tetrahedra (migration step iii of Fig. 5) is not altered by strain; it does not involve bond breaking and does not involve a change in site to site distances.

Experimentally reported values of the migration barrier for proton conductivity in bulk scheelite-type Ca-doped $LaNbO_4$ are close to 0.5 eV,[11,45] in agreement with the values obtained in this study for the unstrained system. Further studies are needed to investigate how extended defects such as dislocations, grain boundaries and space charge regions contribute to the experimentally observed conductivity increase in strained thin films of Ca-doped $LaNbO_4$.[42] We recall that in the Y-doped $BaZrO_3$ proton conductor, it was predicted computationally that lattice strain effects could only account for a limited increase in conductivity.[26] However, epitaxial thin films of Y-doped $BaZrO_3$ showed a major improvement in conductivity compared to the bulk material;[52] such an effect was attributed to the considerable reduction of the grain boundary resistivity in epitaxial strained thin films compared to bulk materials.

4. Conclusions

Previous attempts to improve the proton conductivity of scheelite-type $LaNbO_4$ have focused on doping strategies to increase the oxygen vacancy concentration and thereby the uptake of protonic species, but have proved to be ineffective due to the inherently low dopant solubility. Prompted by the growing interest in lattice strain effects on the properties of a wide range of materials, here we used computational methods to characterize how strain applied to the $LaNbO_4$ SOFC electrolyte material affects doping, defect and proton transport properties.

Four main points emerge:

1. Tensile strain in the *a*–*b* plane improves the solubility of Ca^{2+} dopants, which increases the number of oxygen vacancies, allowing more protons to be accommodated by the structure. The hydration energy is reduced which should further increase the proton uptake. Binding energies of extrinsic defects are lower in strained crystals and might result in less trapping of protons by defect clusters.

2. Tensile strain makes the two most stable proton sites in the structure energetically degenerate and equally likely to be occupied.

3. The anisotropic proton pathways alter from being in the *a*–*b* plane to being in the *a*–*c* plane. This change is rationalized by the reduction in the *c*-lattice parameter and the proton hopping distance as *a*–*b* strain is applied. A small reduction in the migration barrier for the rate determining step is predicted.

4. Compressive strain has the opposite effect on these properties to tensile strain. It reduces dopant solubility, site degeneracy and makes proton migration more anisotropic and should be avoided.

Our results suggest that the application of lattice strain should be regarded as an effective strategy to modulate transport properties where site to site hopping is crucial to conduction (*i.e.* oxide ion or alkali ion conductors). Since proton transport in oxide materials usually requires both site to site hopping and rotation around oxygen sites, the structural modifications induced by lattice strain may not be as effective in the modulation of transport properties.

Acknowledgements

We gratefully acknowledge support from the EPSRC for the Energy Materials Programme grant (EP/K016288), Archer HPC facilities through the Materials Chemistry Consortium (EP/L000202) and the

Italian Ministry of Education, University and Research (MIUR) for the FIRB "Futuro in Ricerca" project INCYPIT (RBFR12CQP5).

References

1 E. Fabbri, D. Pergolesi and E. Traversa, *Chem. Soc. Rev.*, 2010, **39**, 4355–4369.
2 K. D. Kreuer, *Annu. Rev. Mater. Res.*, 2003, **33**, 333–359.
3 L. Malavasi, C. A. J. Fisher and M. S. Islam, *Chem. Soc. Rev.*, 2010, **39**, 4370–4387.
4 D. J. Brett, A. Atkinson, N. P. Brandon and S. J. Skinner, *Chem. Soc. Rev.*, 2008, **37**, 1568–1578.
5 N. M. H. Iwahara, T. Esaka and H. Uchida, *Solid State Ionics*, 1981, **3**, 359–363.
6 K. D. Kreuer, S. Adams, W. Münch, A. Fuchs, U. Klock and J. Maier, *Solid State Ionics*, 2001, **145**, 295–306.
7 A. Magrasò, M. L. Fontaine, Y. Larring, R. Bredesen, G. E. Syvertsen, H. L. Lein, T. Grande, M. Huse, R. Strandbakke, R. Haugsrud and T. Norby, *Fuel Cells*, 2011, **11**, 17–25.
8 R. Haugsrud and T. Norby, *Solid State Ionics*, 2006, **177**, 1129–1135.
9 R. Haugsrud and T. Norby, *Nat. Mater.*, 2006, **5**, 193–196.
10 M. Huse, A. W. B. Skilbred, M. Karlsson, S. G. Eriksson, T. Norby, R. Haugsrud and C. S. Knee, *J. Solid State Chem.*, 2012, **187**, 27–34.
11 Z. Bi, J. Pena-Martìnez, J. H. Kim, C. A. Bridges, A. Huq, J. P. Hodges and M. P. Paranthaman, *Int. J. Hydrogen Energy*, 2012, **37**, 12751–12759.
12 A. D. Brandao, J. Gracio, G. C. Mather, V. V. Kharton and D. P. Fagg, *J. Solid State Chem.*, 2011, **184**, 863–870.
13 M. Ivanova, S. Ricote, W. A. Meulenberg, R. Haugsrud and M. Ziegner, *Solid State Ionics*, 2012, **213**, 45–52.
14 Y. Cao, N. Duan and D. Yan, *J. Solid State Chem.*, 2016, **237**, 248–253.
15 S. Wachowski, A. Mielewczyk-Gryń, K. Zagórski, C. Li, P. Jasiński, S. J. Skinner, R. Haugsrud and M. Gazda, *J. Mater. Chem. A*, 2016, 11696–11707.
16 L. Xiao, D. Mei, M. Cao, D. Qu and B. Deng, *J. Alloys Compd.*, 2015, **627**, 455–462.
17 Y. Cao, N. Duan, X. Wang, B. Chi, J. Pu and L. Jian, *J. Eur. Ceram. Soc.*, 2015, **35**, 1979–1983.
18 K. Wen, W. Lv and W. He, *J. Mater. Chem. A*, 2015, **3**, 20031–20050.
19 A. Kushima and B. Yildiz, *J. Mater. Chem.*, 2010, **20**, 4809.
20 R. A. De Souza, A. Ramadan, S. Hörner and S. Hoerner, *Energy Environ. Sci.*, 2012, **5**, 5445.
21 C. Tealdi and P. Mustarelli, *J. Phys. Chem. C*, 2014, **118**, 29574–29582.
22 N. Schichtel, C. Korte, D. Hesse and J. Janek, *Phys. Chem. Chem. Phys.*, 2009, **11**, 3043–3048.
23 H.-I. Ji, J. Hwang, K. J. Yoon, J.-W. Son, B.-K. Kim, H.-W. Lee and J.-H. Lee, *Energy Environ. Sci.*, 2013, **6**, 116.
24 M. Kubicek, Z. Cai, W. Ma, B. Yildiz, H. Hutter and J. Fleig, *ACS Nano*, 2013, 3276–3286.
25 N. Tsvetkov, Q. Lu, Y. Chen and B. Yildiz, *ACS Nano*, 2015, **9**, 1613–1621.
26 A. Ottochian, G. Dezanneau, C. Gilles, P. Raiteri, C. Knight and J. D. Gale, *J. Mater. Chem. A*, 2014, **2**, 3127.
27 R. Catlow, R. Bell, F. Cora, S. A. French, B. Slater and A. Sokol, *Annu. Rep. Prog. Chem., Sect. A: Inorg. Chem.*, 2005, 513–547.
28 *Computational Approaches to Energy Materials*, ed. A. Walsh, A. A. Sokol and C. R. A. Catlow, Wiley, 2013.
29 J. D. Gale, *J. Chem. Soc., Faraday Trans.*, 1997, **93148**, 629–637.
30 B. G. Dick, Jr. and A. W. Overhauser, *Phys. Rev.*, 1958, **112**, 90–103.
31 N. F. Mott and M. J. Littleton, *Trans. Faraday Soc.*, 1938, **34**, 485–499.
32 G. C. Mather, C. A. J. Fisher and M. S. Islam, *Chem. Mater.*, 2010, **22**, 5912–5917.
33 P. Saul, C. R. A. Catlow and J. Kendrick, *Philos. Mag. B*, 1985, **51**, 107–117.
34 S. J. Stokes and M. S. Islam, *J. Mater. Chem.*, 2010, **20**, 6258.
35 S. Phadke, J. C. Nino and M. S. Islam, *J. Mater. Chem.*, 2012, 25388–25394.
36 P. E. Blöchl, *Phys. Rev. B: Condens. Matter Mater. Phys.*, 1994, **50**, 17953–17979.
37 J. P. Perdew and A. Zunger, *Phys. Rev. B: Condens. Matter Mater. Phys.*, 1981, **23**, 5048–5079.
38 J. Henkelman, P. B. Uberuaga and H. Johnsson, *J. Chem. Phys.*, 2000, **113**, 9901.
39 W. I. F. David, *Mater. Res. Bull.*, 1983, **18**, 749–756.
40 A. Kuwabara, R. Haugsrud, S. Stølen and T. Norby, *Phys. Chem. Chem. Phys.*, 2009, **11**, 5550–5553.
41 C. Tealdi, E. Quartarone, P. Mustarelli and L. Malavasi, *Nanoscale*, 2015, **7**, 2221–2224.
42 A. Cavallaro, C. Solís, P. R. Garcia, B. Ballesteros, J. M. Serra and J. L. Santiso, *Solid State Ionics*, 2012, **216**, 25–30.
43 T. Norby, M. Widerøe, R. Glöckner and Y. Larring, *Dalton Trans.*, 2004, 3012–3018.
44 K. Kreuer, *Solid State Ionics*, 1997, **97**, 1–15.
45 M. Huse, T. Norby and R. Haugsrud, *Int. J. Hydrogen Energy*, 2012, **37**, 8004–8016.
46 J. A. Kilner, *Solid State Ionics*, 2000, **129**, 13–23.
47 M. S. Islam and R. A. Davies, *J. Mater. Chem.*, 2004, **14**, 86.
48 J. A. Dawson and I. Tanaka, *J. Mater. Chem. A*, 2015, **3**, 10045–10051.
49 H. Fjeld, K. Toyoura, R. Haugsrud and T. Norby, *Phys. Chem. Chem. Phys.*, 2010, **12**, 10313–10319.
50 K. Toyoura, N. Hatada, Y. Nose, I. Tanaka, K. Matsunaga and T. Uda, *J. Phys. Chem. C*, 2012, **116**, 19117–19124.
51 K. Nomura and H. Kageyama, *Solid State Ionics*, 2014, **262**, 841–844.
52 D. Pergolesi, E. Fabbri, A. D'Epifanio, E. Di Bartolomeo, A. Tebano, S. Sanna, S. Licoccia, G. Balestrino and E. Traversa, *Nat. Mater.*, 2010, **9**, 846–852.

